Received: 23 July 2024 | Accepted: 12 October 2024

DOI: 10.1111/jopr.13969

ACP AMERICAN COLLEGE OF PROSTHODONTISTS Your smile. Our specialty.

ORIGINAL ARTICLE

Influence of the color of 3D-printed scan aids on the trueness of complete arch digital scans

Özay Önöral DDS, PhD(C) | **Selin Çakır DDS**

Department of Prosthodontics, Faculty of Dentistry, Near East University, Nicosia, Cyprus

Correspondence
Associate Professor Dr Özay Önöral, Department of Prosthodontics, Faculty of Dentistry, Near East University, Nicosia, Mersin 10, Turkey.
Email: [redacted]

Abstract

Purpose: To determine the influence of using 3D-printed scan aids in varying colors on the trueness of digital scans.

Materials and Methods: A master cast with five multi-unit analogues was scanned. The acquired dataset was exported to standard tessellation language (STL) file format to serve as the reference STL. 3D printing of the prototype in five distinct colors (beige [SA^{BEIGE}], grey [SA^{GREY}], white [SA^{WHITE}], red [SA^{RED}], and blue [SA^{BLUE}]) of polylactic acid filament was executed. The experimental STLs of each color group were aligned to the reference STL. RMS values were solely computed for the scan bodies. Based on the centers of the created best-fit and offset planes, scan bodies were converted into virtual cylinders. Cartesian coordinates of each cylinder were acquired. Subsequently, angular (AD) and linear deviation (LD) values were calculated. LD was further examined separately along the x, y, and z axes. Data were statistically analyzed.

Results: According to the results of one-way ANOVAs, significant differences were detected among color groups on AD, LD, RMS estimate error, Δx, Δy, and Δz data. The lowest AD and LD values were exhibited by the SA^{GREY} group in all implant sites. The SA^{GREY} group was followed by the SA^{BEIGE}, SA^{WHITE}, SA^{RED}, and SA^{BLUE} groups.

Conclusions: The SA^{GREY} outperformed the other groups in terms of trueness. Although the LD values of all color groups were below the threshold value (<100 µm), only the AD values of the SA^{GREY}, SA^{BEIGE}, and SA^{WHITE} groups were clinically acceptable (<0.5°).

KEYWORDS
complete arch scans, digital implant impression, impression accuracy, scan aids, superimposition

Misfit of implant-supported fixed dental prostheses is characterized by an irregular and mismatched interface between the implant and the prosthetic superstructure. This misalignment induces static stress not only within the implant components but also in the adjacent bone, ultimately leading to a range of mechanical and biological complications.[1–6] Therefore, accurate recording of the spatial positions of the implants is requisite for the passive fit of implant-supported fixed dental prostheses.[1–4,7–12] This recording can be done by either conventional or digital techniques.[10]

In the conventional technique, open-tray impression copings are prevented from rotational movements through a splinting process (passive stabilization),[11,13] and the impression is subsequently obtained with a custom tray.[14] Although it still offers an acceptable service,[1] it is a time-consuming technique with multiple stages that rely heavily on the operator's skill,[5,10,12,14] and it can be uncomfortable for patients who have a gag reflex or limited mouth opening.[8] Moreover, impression, splinting, and casting materials are dimensionally unstable.[8,9,11,13,15] Accordingly, a digital technique has become popular, circumventing the drawbacks of the conventional technique.[15,16]

In the digital technique, an intraoral scanning (IOS) device and scan bodies are used to transfer the implant positions into

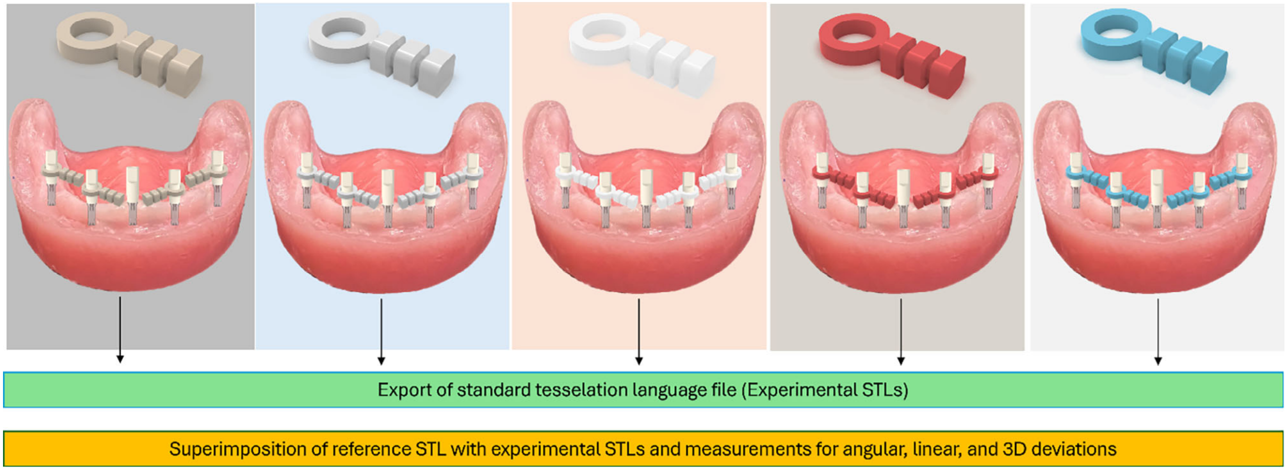

FIGURE 1 Workflow of study.

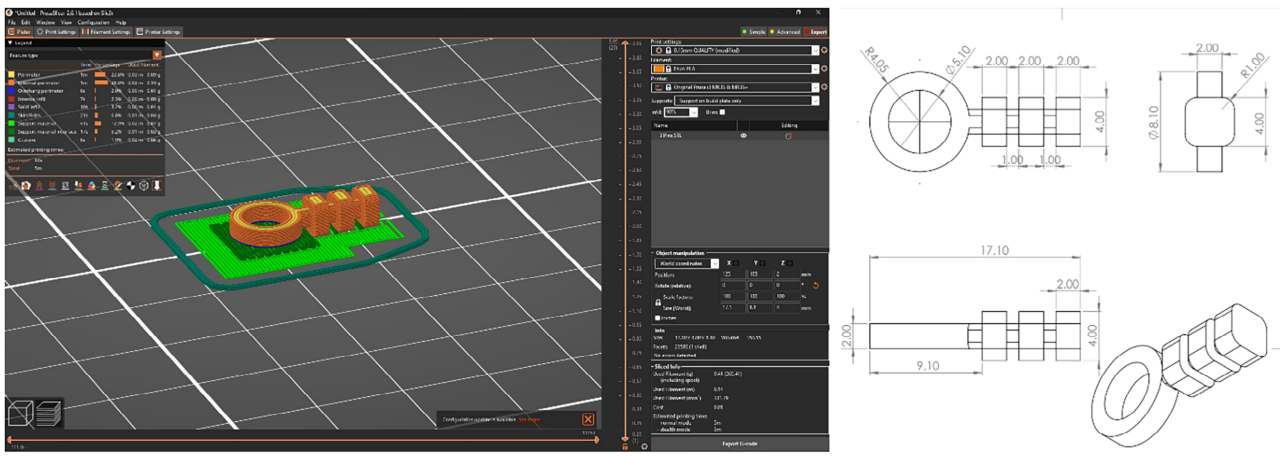

FIGURE 2 3D design of scan aid including dimensions in computer-aided design software package (unit: mm).

a digital environment by capturing raw data in the form of point clouds.[2,3,17] The advantageous features of the IOS technique encompass the elimination of laboratory steps, and the ability to save and store virtual casts in electronic databases, which enhances time efficiency and facilitates better communication with patients.[7,12] Moreover, it is a straightforward technique that enhances patient comfort and satisfaction due to its non-invasive nature.[16] These combined benefits contribute to the growing preference for the IOS technique in clinical settings. IOS devices capture a series of individual images, which are then aligned and combined in sequence by the processing software program using a best-fit alignment algorithm to create a complete and accurate 3D model of the intraoral structures. This process, known as stitching, is facilitated by comprehensive and stable anatomical markers available on the scan path.[6,16,18,19]

Inaccurate stitching adversely influences the accuracy of the digital impression, thereby compromising the passive fit of the implant-supported fixed dental prostheses. Due to the presence of the anatomical markers that assist in the stitching process, it is recommended to use IOS devices only for single-unit and short-span fixed partial restorations.[17,19,20] However, completely edentulous individuals suffer from the lack of anatomical markers and obtaining an accurate scan remains a challenging task.[1,18] Accordingly, the incorporation of artificial markers between scan bodies is suggested.[6,19] Artificial markers extend intentionally towards the edentulous area and provide a continuum by creating an optical bridge between the scan bodies. Thus, it is aimed to compensate or minimize the stitching errors. In previous studies, pressure-indicating paste,[2] fiduciary markers,[2] splinted scan bodies,[13] medicafit plates,[21] splinting frameworks,[22] scan bodies with a lateral flag,[4,12,23] or scan aids positioned on the scan bodies[6,16–18,20] were employed to incorporate the artificial markers. Of these, splinting scan bodies and positioning scan aids on the scan bodies are the most common. The findings of previous studies proved that employing artificial markers accomplishes the intended goal.[19,24] However, the optical quality and geometric features of artificial landmarks are crucial variables that require

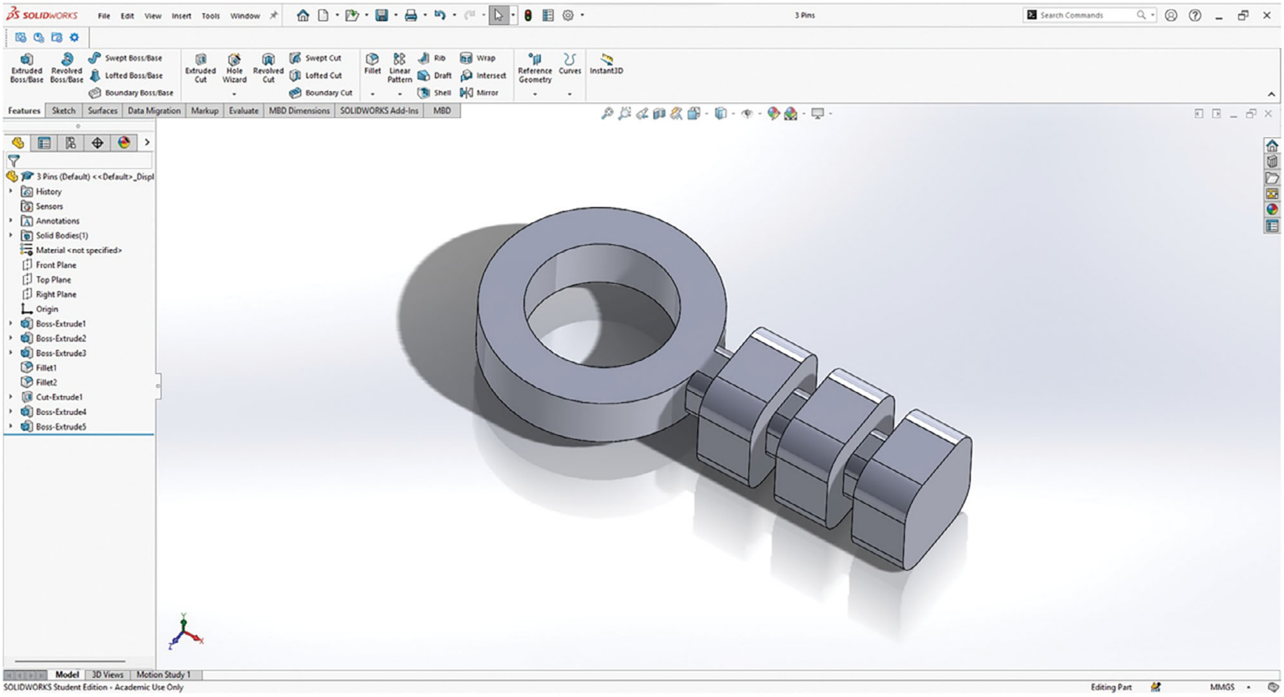

FIGURE 3 Virtually designed scan aid.

careful examination, as they can affect the accuracy of digital scans.[19]

Accuracy is defined as the sum of trueness and precision (ISO 5725-1 and DIN 55350-13). Trueness reflects the impression geometry's divergence from the actual geometry or the similarity of test group datasets to the control group datasets. Precision is the variance between repeated scans or comparisons among test group datasets generated by repeated measurements to evaluate repeatability.[8,15,25] The accuracy of an impression obtained with an IOS device is dependent on operator- and patient-related parameters.[26] The operator-related parameters include IOS technology and system,[27] operator experience,[28] ambient illumination,[29] ambient temperature,[30] scanning head size,[31] scanning strategy,[32] rescanning,[33] cutting off,[34] overlapping,[34] and scanning distance and angulation.[35] The patient-related parameters include arch width,[36] palate features,[37] the quantity of keratinized fixed mucosa,[18] interdental spaces,[38] tooth type,[39] liquid on the tooth surface,[40,41] tooth preparation geometry,[42–44] surface finishing,[45] and existing restorations.[45,46] Additional considerations to be aware of while obtaining digital implant impressions include scan body design,[47] implant depth and angulation,[48] as well as inter-implant distance.[49] Inaccuracies in digital implant impressions become more likely as the inter-implant distance gets longer, possibly due to accumulative faults in the IOS stitching process. In a systematic review,[50] 16–22 mm was reported as acceptable thresholds of inter-implant distance for accurate complete arch scans.

The accuracy of the IOS device cannot be fully assessed without a meticulous analysis of the substrates being scanned. The intrinsic physical properties of a substrate significantly influence the reflection of light from its surface.[25] Parameters such as reflectivity, refractive index, and translucency of a substrate modulate the amount of light received by the sensor of the IOS device, thereby affecting the accuracy of the 3-dimensional (3D) data captured.[5,25,51] A recent study[52] reported 100 µm and 0.5° as acceptable threshold values for linear and angular distortion in completely edentulous arches, although consensus on these thresholds remains unclear.

Not only are studies reporting the effect of scan aids with different geometries on impression accuracy scarce, but there is also only one study[20] evaluating the influence of the color of scan aids on impression accuracy to the best knowledge of the authors. Therefore, the purpose of this study was to evaluate the effect of using 3D-printed scan aids in varying colors (SA^{BEIGE}, SA^{GREY}, SA^{WHITE}, SA^{RED}, and SA^{BLUE}) on the trueness of digital scans. The null hypothesis was that the trueness values of the digital scans obtained with scan aids in varying colors would not be significantly different.

MATERIALS AND METHODS

The flowchart of this study is depicted in Figure 1. A power analysis was conducted to determine the required sample size, which was calculated by employing a statistical analysis software package (G*Power 3.1.9.7; Heinrich-Heine-Universität Düsseldorf). To achieve 85% power with an effect size of 0.25 at $\alpha = 0.05$, 15 scans were needed for each experimental group.

A master cast of an edentulous mandible with 5 multi-unit analogues (T0 32202; NucleOSS) was made, sprayed with an antireflective powder spray (3D Scanning Spray;

TABLE 1 Results of one-way ANOVAs.

	Factor	Type III sum of squares	*df*	Mean square	*F*	*p*
Angular deviation data of #45	Between groups	6.748	4	1.687	967.162	<0.001
	Within groups	.122	70	.002		
	Total	6.870	74			
Angular deviation data of #43	Between groups	10.967	4	2.742	1178.830	<0.001
	Within groups	.163	70	.002		
	Total	11.130	74			
Angular deviation data of #41-31	Between groups	12.977	4	3.244	637.251	<0.001
	Within groups	.356	70	.005		
	Total	13.334	74			
Angular deviation data of #33	Between groups	14.327	4	3.582	855.145	<0.001
	Within groups	.293	70	.004		
	Total	14.620	74			
Angular deviation data of #35	Between groups	15.191	4	3.798	628.428	<0.001
	Within groups	.423	70	.006		
	Total	15.614	74			
Linear deviation data of #45	Between groups	2007.191	4	183.222	8.891	<0.001
	Within groups	34.609	70	20.608		
	Total	2041.800	74			
Linear deviation data of #43	Between groups	3043.330	4	760.833	1011.614	<0.001
	Within groups	52.647	70	.752		
	Total	3095.977	74			
Linear deviation data of #41-31	Between groups	3910.753	4	977.688	598.181	<0.001
	Within groups	114.411	70	1.634		
	Total	4025.163	74			
Linear deviation data of #33	Between groups	4323.203	4	1080.801	844.555	<0.001
	Within groups	89.581	70	1.280		
	Total	4412.784	74			
Linear deviation data of #35	Between groups	4584.330	4	1146.082	631.042	<0.001
	Within groups	127.132	70	1.816		
	Total	4711.462	74			
RMS data	Between groups	6.967	4	1.742	2547.284	<0.001
	Within groups	.048	70	.001		
	Total	7.015	74			

Bilkim Co. Ltd.), and then scanned using a benchtop extraoral scanner (inEOS X5; Dentsply Sirona) upon fastening scan bodies (T0 32033; NucleOSS) to the multi-unit analogues at 10 Ncm with a manual torque wrench. The acquired dataset was exported to standard tessellation language (STL) file format to be used as the reference STL.

A scan aid consisting of collar and lateral extension components was virtually designed using a software program (SolidWorks; Dassault Systèmes Corp) (Figures 2 and 3). The collar was engineered to be sufficiently tight for retention on the scan bodies by tolerance. 3D printing of the prototype in five distinct colors (beige, grey, white, red, and blue) of polylactic acid filament (PLA plus; Esun Industrial Co.) was executed on a fused deposition modeling machine (Prusa MK3S; Prusa Research A.S.) with a print nozzle temperature of 210°C and a print bed temperature of 60°C.

Firstly, five SBs were screwed to the multiunit analogues in the master cast at 10 Ncm with a manual torque wrench, and the scan aids manufactured in beige color were friction-attached to the scan bodies. Accordingly, 15 consecutive scans were performed using an intraoral digitizer (CEREC Omnicam; Dentsply Sirona, Software version: CEREC SW 4.5) functioning with optical triangulation technology. The scanning protocol was initiated at implant site 45 and executed by a single calibrated operator. Following the manufacturer's endorsement, a standardized scan trajectory

TABLE 2 Descriptive statistics for angular deviation values with pairwise comparisons.

				95% Confidence interval					
Implant site	**Color of scan aid**	**Mean**	**±SD**	**Lower bound**	**Upper bound**	**Median**	**IQR**	**Sig.***	***p* values**
45	Grey	0.12	0.04	0.10	0.14	0.12	0.07	A	SA^{GREY} versus SA^{BEIGE}: $p = 0.202$
	Blue	0.91	0.05	0.88	0.93	0.91	0.07	D	Remaining comparisons: $p < 0.001$
	Beige	0.15	0.04	0.13	0.17	0.14	0.06	A	
	Red	0.56	0.05	0.54	0.59	0.55	0.07	C	
	White	0.24	0.03	0.22	0.25	0.24	0.05	B	
43	Grey	0.13	0.03	0.11	0.15	0.13	0.06	A	SA^{GREY} versus SA^{BEIGE}: $p = 0.110$
	Blue	1.14	0.08	1.10	1.18	1.12	0.08	D	Remaining comparisons: $p < 0.001$
	Beige	0.17	0.02	0.16	0.18	0.17	0.03	A	
	Red	0.68	0.06	0.64	0.71	0.70	0.11	C	
	White	0.28	0.04	0.26	0.30	0.27	0.03	B	
Between 41 and 31	Grey	0.21	0.05	0.18	0.24	0.21	0.07	A	SA^{GREY} versus SA^{BEIGE}: $p = 0.217$
	Blue	1.32	0.12	1.25	1.39	1.31	0.19	D	Remaining comparisons: $p < 0.001$
	Beige	0.27	0.05	0.24	0.29	0.27	0.06	A	
	Red	0.81	0.07	0.78	0.85	0.82	0.07	C	
	White	0.41	0.02	0.39	0.42	0.41	0.04	B	
33	Grey	0.22	0.06	0.19	0.25	0.20	0.10	A	SA^{GREY} versus SA^{BEIGE}: $p = 0.006$
	Blue	1.39	0.09	1.34	1.44	1.36	0.15	E	Remaining comparisons: $p < 0.001$
	Beige	0.30	0.04	0.28	0.32	0.30	0.06	B	
	Red	0.89	0.08	0.84	0.93	0.86	0.09	D	
	White	0.44	0.05	0.41	0.46	0.42	0.11	C	
	Grey	0.25	0.04	0.22	0.27	0.23	0.08	A	SA^{GREY} versus SA^{BEIGE}: $p = 0.017$
	Blue	1.45	0.15	1.37	1.53	1.49	0.28	E	Remaining comparisons: $p < 0.001$
35	Beige	0.34	0.04	0.31	0.36	0.33	0.07	B	
	Red	0.97	0.05	0.94	0.99	0.97	0.08	D	
	White	0.49	0.04	0.46	0.51	0.48	0.06	C	

was adopted, which began with scanning the occlusal surface, then the buccal surface, and finally the lingual surface. Each scanning session was monitored, and a scan was deemed complete when all of the scan body surfaces were recorded and no major gaps in the virtual model were present. The acquired datasets were exported to be used as experimental STLs of the beige group. The above-mentioned stages were repeated for other color groups.

All STLs were uploaded to inspection software package (Geomagic Control X; 3D systems). The experimental STLs of each color group were aligned to the reference STL by running the best-fit alignment command. While executing this command, scan bodies were omitted, and only stable regions, such as ridges, were used to minimize error. The 3D comparison algorithm was utilized for generating colorimetric mappings of 3D deviations (max/min critical: ±100 µm, max/min nominal: ±50 µm) as well as for determining the root mean square estimate error (RMS), a numerical measure of how well the datasets matched. RMS values were solely computed for the scan bodies, not the complete cast, through the compare-selection tab. In continuation, best-fit planes were created on the occlusal surfaces of the scan bodies by using the create feature command. Offset planes were created 10 mm away from the best-fit planes. Based on the centers of best-fit and offset planes, scan bodies were converted into hollow virtual cylinders that mimic the dimensional properties (height and diameter) of the scan bodies. By utilizing the create annotations command in the compare features tab, Cartesian coordinates of each cylinder in the reference STL were acquired, as well as those in the experimental STL (Figure 4). Subsequently, angular (AD) and linear deviation (LD) values were calculated by using the following mathematical equations:

$$\mathrm{LD} = \sqrt{\left((X_1 - X_2)^2 + (Y_1 - Y_2)^2 + (Z_1 - Z_2)^2\right)}$$

$$\mathrm{AD} = \left(\arccos\left[\left((\mathrm{X}_1 \times \mathrm{X}_2) + (\mathrm{Y}_1 \times \mathrm{Y}_2) + (\mathrm{Z}_1 \times \mathrm{Z}_2)\right) / \left(\sqrt{\left(X_1^2 + Y_1^2 + Z_1^2\right)} \times \sqrt{\left(X_2^2 + Y_2^2 + Z_2^2\right)}\right)\right]\right)$$

The reference cylinder's center line is represented by Cartesian coordinates X_1, Y_1, and Z_1, while the experimental cylinder's center line is represented by Cartesian coordinates X_2, Y_2, and Z_2.

Only the size was considered for the AD and LD values. At each site, LD was further examined separately along the x, y, and z axes to assess both the direction and extent of deviation in these axes (Δx, Δy, and Δz). These represent the raw data indicating the direction of the deviation. However, absolute values were used for statistical analysis.

All statistical analyses were executed through a software program (SPSS Statistics 25.0, SPSS Inc.). The Shapiro–Wilk test showed that the data were normally distributed ($p > 0.05$). One-way analysis of variances (ANOVA) was used to determine significant differences in LD, AD, RMS, Δx, Δy, and Δz values among all groups. Tukey's HSD was used for post-hoc comparisons among groups ($\alpha = 0.05$).

RESULTS

In accordance with the results of one-way ANOVAs, significant differences were detected among color groups on AD, LD, and RMS estimate error data in all implant sites (Table 1). Tables 2 and 3 show the mean AD and LD values with Tukey post hoc comparisons. The lowest AD and LD values were exhibited by the SA^{GREY} group in all implant sites. The SA^{GREY} group was followed by the SA^{BEIGE}, SA^{WHITE}, SA^{RED}, and SA^{BLUE} groups. In implant sites 33 and 35, statistically significant difference was detected between the SA^{GREY} and SA^{BEIGE} groups ($p < 0.05$). However, in the remaining implant sites, the difference between the SA^{GREY} and SA^{BEIGE} groups was not statistically significant ($p > 0.05$). All pairwise comparisons among SA^{BEIGE}, SA^{WHITE}, SA^{RED}, and SA^{BLUE} groups were statistically significant ($p < 0.05$). Although the LD values of all color groups were below the threshold value (<100 μm); only the

TABLE 3 Descriptive statistics for linear deviation values with pairwise comparisons.

				95% Confidence interval					
Implant site	Color of scan aid	Mean	±SD	Lower bound	Upper bound	Median	IQR	Sig.*	*p* values
45	Grey	2.30	0.57	1.99	2.62	2.31	0.92	A	SA^{GREY} versus SA^{BEIGE}: $p = 0.099$ Remaining comparisons: $p < 0.001$
	Blue	15.92	0.89	15.43	16.42	15.96	0.72	D	
	Beige	2.95	0.63	2.60	3.30	2.88	0.92	A	
	Red	9.89	0.86	9.41	10.36	9.58	1.12	C	
	White	4.28	0.46	4.03	4.54	4.31	0.86	B	
43	Grey	3.12	0.51	2.83	3.40	3.13	0.72	A	SA^{GREY} versus SA^{BEIGE}: $p = 0.161$ Remaining comparisons: $p < 0.001$
	Blue	19.92	1.33	19.19	20.66	19.56	1.49	D	
	Beige	3.84	0.29	3.68	4.00	3.76	0.46	A	
	Red	12.13	1.16	11.49	12.77	12.56	2.25	C	
	White	5.44	0.56	5.13	5.75	5.30	0.75	B	
Between 41-31	Grey	3.72	0.83	3.26	4.18	3.75	1.42	A	SA^{GREY} versus SA^{BEIGE}: $p = 0.113$ Remaining comparisons: $p < 0.001$
	Blue	23.09	2.15	21.90	24.29	22.88	3.41	D	
	Beige	4.86	0.91	4.36	5.37	5.12	0.51	A	
	Red	14.32	1.25	13.63	15.01	14.39	1.67	C	
	White	7.34	0.68	6.97	7.72	7.16	0.89	B	
33	Grey	3.86	0.99	3.32	4.41	3.56	1.67	A	SA^{GREY} versus SA^{BEIGE}: $p = 0.004$ Remaining comparisons: $p < 0.001$
	Blue	24.25	1.58	23.37	25.13	23.78	2.64	E	
	Beige	5.40	0.74	4.99	5.81	5.25	1.03	B	
	Red	15.50	1.32	14.77	16.23	15.03	1.57	D	
	White	7.72	0.80	7.28	8.16	7.51	1.51	C	
	Grey	4.45	0.73	4.04	4.85	4.17	1.42	A	SA^{GREY} versus SA^{BEIGE}: $p = 0.025$ Remaining comparisons: $p < 0.001$
	Blue	25.28	2.60	23.84	26.72	25.96	4.88	E	
35	Beige	5.95	0.70	5.57	6.34	5.77	1.11	B	
	Red	16.89	0.86	16.41	17.36	16.91	1.43	D	
	White	8.53	0.73	8.12	8.93	8.57	0.93	C	

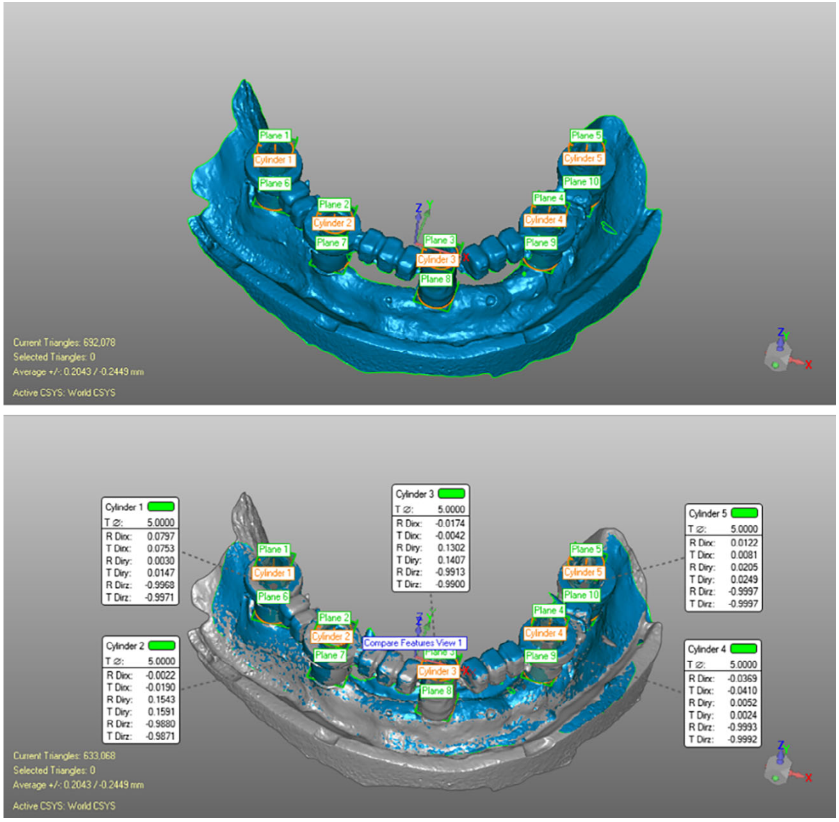

FIGURE 4 Superimposition of reference and experimental STL files to record Cartesian coordinates.

TABLE 4 Descriptive statistics for RMS values with pairwise comparisons.

Color of scan aid	Mean	±SD	95% Confidence interval		Median	IQR	Sig.*	p values
			Lower bound	Upper bound				
Grey	0.343	0.04	0.32	0.36	0.34	0.06	A	For all comparisons: $p < 0.001$
Blue	1.134	0.03	1.12	1.15	1.12	0.04	E	
Beige	0.442	0.02	0.43	0.45	0.44	0.04	B	
Red	0.985	0.01	0.98	0.99	0.98	0.02	D	
White	0.661	0.03	0.65	0.68	0.67	0.05	C	

AD values of the SA^{GREY}, SA^{BEIGE}, and SA^{WHITE} groups were clinically acceptable (<0.5°).

Table 4 depicts the mean RMS values with Tukey post hoc comparisons. The SA^{BLUE} group had the highest mean RMS value, followed by SA^{RED}, SA^{WHITE}, SA^{BEIGE}, and SA^{GREY} groups. Differences among all color groups were statistically significant ($p < 0.01$).

According to the results of one-way ANOVAs, Δx, Δy, and Δz values differed significantly among color groups in all implant sites, except for Δz values in implant site 33. Figure 5 shows the Box and Whisker charts for the Δx (+ → mesial shift, − → distal shift), Δy (+ → lingual shift, − → buccal shift), and Δz values (+ → occlusal shift, − → gingival shift). The highest and the lowest LD values were observed on the x-axis and z-axis, respectively (Tables 5–7). Except for Δx values in implant site 35, The SA^{BLUE} group exhibited the highest Δx and Δy values across all implant sites, followed by the SA^{RED} group (Tables 5–6). It was also found that each implant site had a different group showing the highest Δz values (Table 7).

DISCUSSION

This study analyzed the scan trueness by using one IOS system with 3D-printed scan aids in varying colors. The null hypothesis was rejected as significant differences were detected among the scan aids in varying colors.

IOS devices collect data by detecting the light reflected off the scanned substrate. The way light reflects off different substrates varies depending on the color and texture of those substrates.[15] For instance, when scanning glossy or translucent substrates, such as enamel shade composite, natural enamel, metals, and high translucent feldspathic

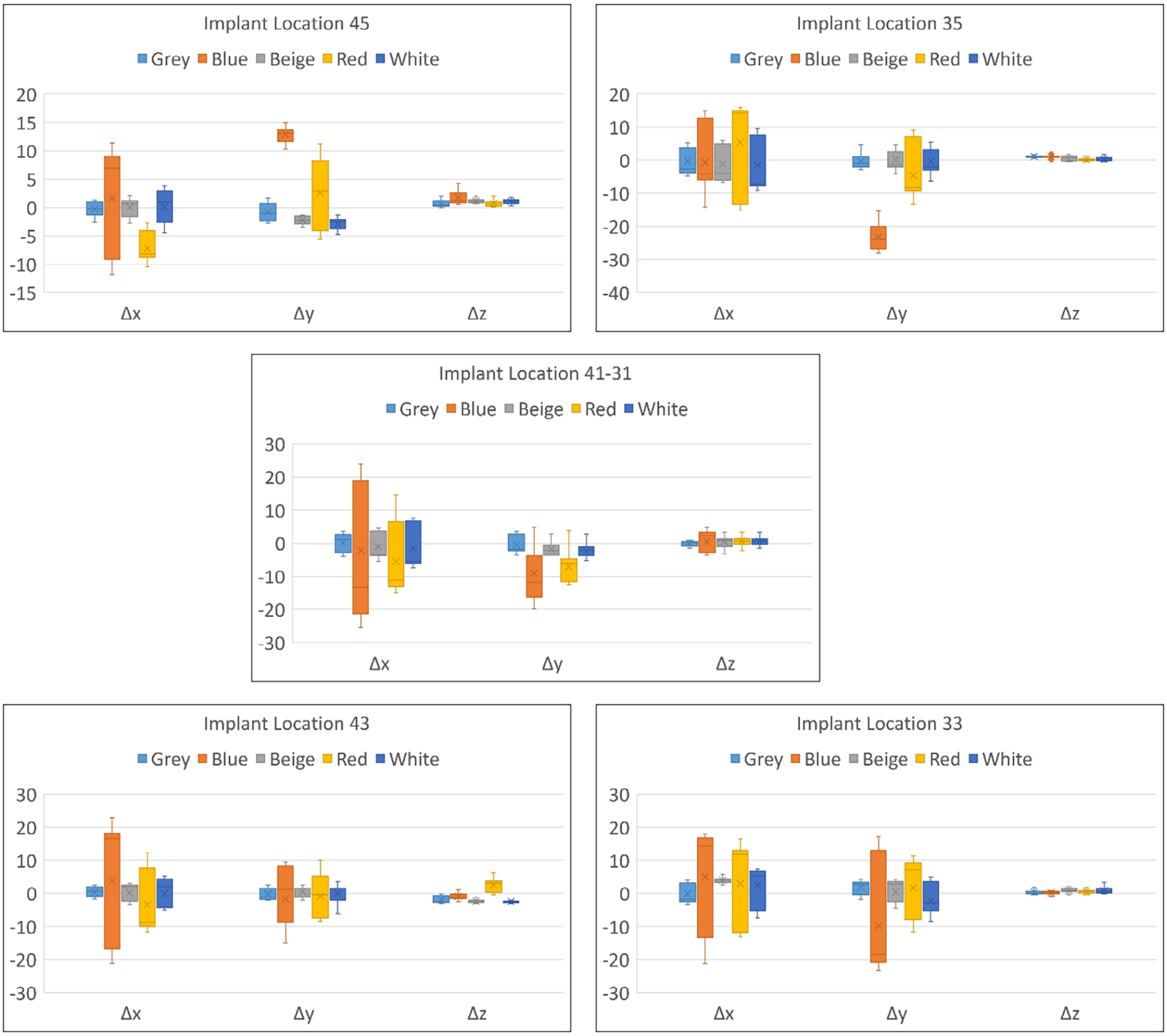

FIGURE 5 Box and whisker charts for Δx, Δy, and Δz values (Δx, distortion in mesiodistal direction [+ → mesial shift, – → distal shift]; Δy; distortion in buccolingual direction [+ → lingual shift, – → buccal shift]; Δz, distortion in occluso-gingival direction [+ → occlusal shift, – → gingival shift]) (unit: µm).

ceramics, the reflected light signals can become distorted due to multiple scattering or indirect illumination, complicating depth estimations and adversely influencing the scan accuracy.[5,6,19,46] Supportively, in a study by Elter and Tak,[51] natural enamel and metal surfaces exhibited the lowest trueness values, respectively. The authors linked these results to the idea that metal surfaces, which reflect more light, can result in errors in how reflected light is processed, and that natural enamel, possessing high translucency, induces multiple scattering. The authors also stated that the opalescence and fluorescence features of natural teeth may alter the optical behavior of the light, thereby influencing the scan accuracy.[51] Besides the substrate's translucency, its thickness also affects how light behaves. For instance, enamel-like trueness is normally expected in feldspathic ceramics that replicate the optical properties of the enamel tissue. However, it is also possible that the feldspathic ceramic may show better trueness than enamel tissue as a result of increasing its thickness and therefore decreasing its translucency, as reported in a previous study.[51] Contrastingly, substrates like dentine shade composite, natural dentine, and zirconia ceramics have less of a negative impact on scanning accuracy compared to glossy or translucent substrates.[5,51] Although natural dentin can vary in refractive index depending on how the tubules are oriented in the scan area,[5,15] it has a lower refractive index than enamel, thereby causing IOS devices to operate more accurately.[15,51]

According to the results of this study, the highest distortion values were recorded in the SA$^{\text{BLUE}}$ group. To the best knowledge of the authors, no study is available to compare this finding directly. However, a recent study by Dutton et al.[46] tested whether material substrates affect the accuracy of intraoral scanners, and high deviation values were observed in the blue core substrate in the Omnicam-scanned

TABLE 5 Descriptive statistics for Δx values (μm) with pairwise comparisons.

Implant location	Color of scan aid	Mean ± SD	95% Confidence interval Lower bound	Upper bound	Sig.*	p values
45	Grey	1.23 ± 0.59	0.90	1.56	A	SA^{GREY} versus SA^{BEIGE}: $p = 1.000$ SA^{GREY} versus SA^{WHITE}: $p = 0.241$ SA^{BLUE} versus SA^{RED}: $p = 0.076$ SA^{BEIGE} versus SA^{WHITE}: $p = 0.311$ Remaining comparisons: $p < 0.001$
	Blue	8.80 ± 2.05	7.66	9.94	B	
	Beige	1.32 ± 0.63	0.97	1.67	A	
	Red	7.25 ± 2.58	5.82	8.68	B	
	White	2.46 ± 1.20	1.80	3.12	A	
43	Grey	1.32 ± 0.70	0.93	1.71	A	SA^{GREY} versus SA^{BEIGE}: $p = 0.251$ SA^{BEIGE} versus SA^{WHITE}: $p = 0.017$ Remaining comparisons: $p < 0.001$
	Blue	17.79 ± 2.54	16.38	19.20	D	
	Beige	2.43 ± 0.64	2.08	2.79	A	
	Red	9.35 ± 1.69	8.42	10.29	C	
	White	4.17 ± 0.87	3.68	4.65	B	
41–31	Grey	2.58 ± 1.08	1.98	3.18	A	SA^{GREY} versus SA^{BEIGE}: $p = 0.741$ SA^{BEIGE} versus SA^{WHITE}: $p = 0.021$ Remaining comparisons: $p < 0.001$
	Blue	19.40 ± 4.17	17.09	21.71	D	
	Beige	3.66 ± 0.89	3.17	4.16	A	
	Red	11.15 ± 3.05	9.46	12.84	C	
	White	6.44 ± 0.91	5.94	6.94	B	
33	Grey	2.72 ± 0.76	2.30	3.14	A	SA^{GREY} versus SA^{BEIGE}: $p = 0.230$ SA^{BEIGE} versus SA^{WHITE}: $p = 0.036$ Remaining comparisons: $p < 0.001$
	Blue	15.59 ± 2.79	14.05	17.14	D	
	Beige	4.00 ± 0.87	3.52	4.48	A	
	Red	12.47 ± 1.69	11.53	13.40	C	
	White	5.78 ± 1.39	5.01	6.55	B	
35	Grey	3.76 ± 0.68	3.38	4.14	A	SA^{GREY} versus SA^{BEIGE}: $p = 0.574$ SA^{BLUE} versus SA^{BEIGE}: $p = 0.006$ SA^{BLUE} versus SA^{WHITE}: $p = 0.941$ SA^{BEIGE} versus SA^{WHITE}: $p = 0.053$ Remaining comparisons: $p < 0.001$
	Blue	8.33 ± 5.02	5.56	11.11	B	
	Beige	5.11 ± 1.21	4.44	5.78	AB	
	Red	14.14 ± 1.75	13.17	15.11	C	
	White	7.64 ± 0.97	7.11	8.17	B	

group. This finding provides consistency with that of the current study and indicates that Omnicam device functioning with optical triangulation technology is inferior in terms of perception algorithm of blue color. Moreover, in the same study,[46] PrimeScan, the newer version of Omnicam device functioning with confocal microscopy technology, exhibited the lowest deviation values for blue core substrate. It can be inferred that the perception of blue color has been enhanced in the newer version. The SA^{BLUE} group was followed by the SA^{RED} group. It is possible that the scanner's algorithm struggled to differentiate between the red scan aid and the pink acrylic resin used to simulate gingival areas, which could have adversely influenced the scanning trueness.

The SA^{GREY} group outperformed the other groups in the current study. This performance of the SA^{GREY} group can be attributed to the achromatic nature of grey color. When white light interacts with a grey surface, part of the light is absorbed while the rest is reflected. However, the amount of light absorbed versus reflected is dependent on the shade of grey. As more light is absorbed, the grey becomes darker; while increased reflection makes the grey lighter. In the SA^{GREY} group, light grey PLA filament was used. For this reason, there may have been more reflection from the light grey substrate to the IOS sensor, which may have increased the accuracy. In contrast, Kernen et al reported that the auxiliary device in beige color demonstrated higher trueness than that in the grey color. However, a very dark gray was preferred and this may have reduced the amount of light reflected back to the sensor. Although a direct comparison and an inference cannot be made, polished amalgam depicting a light grey surface was among the top 3 substrates offering the highest scanning trueness for the Omnicam device in a recent study.[46] The SA^{GREY} group was followed by the SA^{BEIGE} group in this study. It may be stated that the Omnicam device functioning with confocal microscopy technology perceives the grey color better. And the beige color may be optimal for the active-triangulation acquisition technology, as reported by Wu et al.[19]

The SA^{WHITE} group did not perform as truly as groups SA^{GREY} and SA^{BEIGE}. Coherently, Kernen et al.[20] found that white scan aids had lower trueness than beige and grey scan aids. For the SA^{WHITE} group, translucent white PLA

TABLE 6 Descriptive statistics for Δy values (μm) with pairwise comparisons.

Implant location	Color of scan aid	Mean ± SD	95% Confidence interval		Sig.*	*p* values
			Lower bound	Upper bound		
45	Grey	1.57 ± 0.75	1.15	1.98	A	SA^{GREY} versus SA^{BEIGE}: $p = 0.765$ SA^{GREY} versus SA^{WHITE}: $p = 0.103$ SA^{BEIGE} versus SA^{WHITE}: $p = 0.681$ Remaining comparisons: $p < 0.001$
	Blue	12.92 ± 1.36	12.17	13.67	C	
	Beige	2.23 ± 0.74	1.81	2.64	A	
	Red	5.63 ± 2.78	4.09	7.17	B	
	White	2.97 ± 1.06	2.38	3.55	A	
43	Grey	1.68 ± 0.44	1.44	1.92	A	SA^{GREY} versus SA^{BEIGE}: $p = 1.000$ SA^{GREY} versus SA^{WHITE}: $p = 0.995$ SA^{BLUE} versus SA^{RED}: $p = 0.501$ SA^{BEIGE} versus SA^{WHITE}: $p = 0.986$ Remaining comparisons: $p < 0.001$
	Blue	7.67 ± 4.08	5.41	9.93	B	
	Beige	1.58 ± 0.45	1.33	1.83	A	
	Red	6.31 ± 2.88	4.72	7.91	B	
	White	2.01 ± 1.30	1.29	2.73	A	
41–31	Grey	2.27 ± 0.96	1.73	2.80	A	SA^{GREY} versus SA^{BEIGE}: $p = 1.000$ SA^{GREY} versus SA^{WHITE}: $p = 0.992$ SA^{BLUE} versus SA^{RED}: $p = 0.283$ SA^{BEIGE} versus SA^{WHITE}: $p = 0.995$ Remaining comparisons: $p < 0.001$
	Blue	10.02 ± 6.11	6.64	13.40	B	
	Beige	2.35 ± 1.21	1.68	3.01	A	
	Red	7.59 ± 3.79	5.49	9.69	B	
	White	2.81 ± 1.39	2.04	3.58	A	
33	Grey	2.51 ± 1.11	1.89	3.12	A	SA^{GREY} versus SA^{BEIGE}: $p = 0.801$ SA^{GREY} versus SA^{WHITE}: $p = 0.067$ SA^{BEIGE} versus SA^{WHITE}: $p = 0.521$ Remaining comparisons: $p < 0.001$
	Blue	18.11 ± 3.52	16.17	20.06	C	
	Beige	3.34 ± 0.78	2.91	3.77	A	
	Red	8.92 ± 1.94	7.84	10.00	B	
	White	4.52 ± 1.79	3.53	5.51	A	
35	Grey	1.76 ± 1.21	1.09	2.42	A	SA^{GREY} versus SA^{BEIGE}: $p = 0.877$ SA^{GREY} versus SA^{WHITE}: $p = 0.302$ SA^{BEIGE} versus SA^{WHITE}: $p = 0.855$ Remaining comparisons: $p < 0.001$
	Blue	23.12 ± 4.21	20.79	25.45	C	
	Beige	2.55 ± 1.05	1.96	3.13	A	
	Red	8.90 ± 1.94	7.83	9.97	B	
	White	3.38 ± 1.44	2.58	4.18	A	

filament was preferred. This finding is likely because the Omnicam, which utilizes unpolarized white light for data collection, may have encountered difficulty scanning the translucent white substrate and this may have complicated the scanning process. Translucent white materials scatter the incoming white light in multiple directions. As a result of the scattering, the light that passes through the translucent white material emerges with a softened and diffused appearance. This diffused light lacks sharp boundaries and tends to spread out, creating a gentle glow rather than distinct beams of light. It can be inferred that translucent white substrate causes IOS devices to operate less accurately due to the less reflected light beam.[24]

In this study, where LD was evaluated separately for each Cartesian coordinate, the highest deviation values were observed on the x-coordinate. Based on this, it can be stated that the scan aids underwent the highest positional deformation in the mesio-distal direction. This situation may be related to the chosen scan trajectory. The scanner head captured the tissues by moving in the disto-mesial direction. If a zig-zag scan trajectory had been chosen, the adverse influence could have been reflected in other axes.

Limitations of this study include the in vitro experimental design, the scanning protocol, and the IOS technologies. The presence of saliva or moisture, as well as variations in ambient lighting conditions, can all influence the results. The clinical acceptance could be further validated by fabricating a bar for all-on-5 restoration and assessing its actual fit. The image acquisition principle for Omnicam is active triangulation. Dutton et al[46] reported that confocal microscopy IOS devices seem to be less sensitive to substrate variations compared to active triangulation scanners. Using different IOS technologies and scan strategies can change the results. Therefore, further studies are needed.

CONCLUSIONS

Although the linear deviation values of all groups were well below the threshold value (<100 μm), only the angular distortion values of the scan bodies used with grey, beige, and white scan aids were clinically acceptable (<0.5°). The digital impressions obtained by grey scan aids outperformed the other color groups.

TABLE 7 Descriptive statistics for Δz values (μm) with pairwise comparisons.

Implant location	Color of scan aid	Mean ± SD	95% Confidence interval Lower bound	95% Confidence interval Upper bound	Sig.*	*p* values
45	Grey	0.68 ± 0.57	0.36	1.00	A	SA^{GREY} versus SA^{BEIGE}: $p = 0.329$; SA^{GREY} versus SA^{RED}: $p = 1.000$ SA^{GREY} versus SA^{WHITE}: $p = 0.565$; SA^{BLUE} versus SA^{BEIGE}: $p = 0.178$ SA^{BLUE} versus SA^{WHITE}: $p = 0.075$; SA^{BEIGE} versus SA^{RED}: $p = 0.433$ SA^{BEIGE} versus SA^{WHITE}: $p = 0.995$; SA^{RED} versus SA^{WHITE}: $p = 0.682$ Remaining comparisons: $p < 0.001$
	Blue	1.73 ± 1.19	1.07	2.38	B	
	Beige	1.16 ± 0.38	0.95	1.37	AB	
	Red	0.73 ± 0.57	0.41	1.04	A	
	White	1.06 ± 0.44	0.82	1.30	AB	
43	Grey	1.93 ± 1.06	1.34	2.52	AB	SA^{GREY} versus SA^{BLUE}: $p = 0.261$; SA^{GREY} versus SA^{BEIGE}: $p = 0.760$; SA^{GREY} versus SA^{RED}: $p = 0.238$; SA^{GREY} versus SA^{WHITE}: $p = 0.610$; SA^{BLUE} versus SA^{BEIGE}: p=0.016; SA^{BLUE} versus SA^{WHITE}: $p = 0.008$; SA^{BEIGE} versus SA^{RED}: p=0.895; SA^{BEIGE} versus SA^{WHITE}: $p = 0.999$; SA^{RED} versus SA^{WHITE}: $p = 0.965$; Remaining comparisons: p<0.001
	Blue	1.16 ± 0.66	0.80	1.52	A	
	Beige	2.37 ± 0.50	2.10	2.65	B	
	Red	2.71 ± 1.84	1.69	3.74	B	
	White	2.47 ± 0.33	2.28	2.65	B	
41-31	Grey	0.71 ± 0.49	0.44	0.99	A	SA^{GREY} versus SA^{BEIGE}: $p = 0.081$; SA^{GREY} versus SA^{RED}: $p = 0.515$ SA^{GREY} versus SA^{WHITE}: $p = 0.502$; SA^{BEIGE} versus SA^{RED}: $p = 0.846$ SA^{BEIGE} versus SA^{WHITE}: $p = 0.855$; SA^{RED} versus SA^{WHITE}: $p = 1.000$ Remaining comparisons: $p < 0.001$
	Blue	3.02 ± 0.87	2.53	3.50	B	
	Beige	1.55 ± 1.05	0.96	2.13	A	
	Red	1.22 ± 0.89	0.73	1.71	A	
	White	1.23 ± 0.97	0.69	1.76	A	
33	Grey	0.56 ± 0.43	0.32	0.80	A	No statistically significant difference among groups ($p = 0.135$)
	Blue	0.47 ± 0.27	0.32	0.62	A	
	Beige	0.93 ± 0.60	0.60	1.26	A	
	Red	0.67 ± 0.49	0.40	0.94	A	
	White	0.89 ± 0.92	0.38	1.40	A	
35	Grey	1.07 ± 0.33	0.89	1.26	C	SA^{GREY} versus SA^{BLUE}: $p = 0.995$; SA^{GREY} versus SA^{BEIGE}: $p = 0.591$ SA^{GREY} versus SA^{WHITE}: $p = 0.040$; SA^{BLUE} versus SA^{BEIGE}: $p = 0.818$ SA^{BLUE} versus SA^{RED}: $p = 0.005$; SA^{BLUE} versus SA^{WHITE}: $p = 0.102$ SA^{BEIGE} versus SA^{RED}: $p = 0.094$; SA^{BEIGE} versus SA^{WHITE}: $p = 0.615$ SA^{RED} versus SA^{WHITE}: $p = 0.798$; Remaining comparisons: $p < 0.001$
	Blue	1.01 ± 0.56	0.70	1.32	BC	
	Beige	0.82 ± 0.47	0.56	1.08	ABC	
	Red	0.38 ± 0.43	0.14	0.62	A	
	White	0.57 ± 0.54	0.27	0.87	AB	

ORCID

Özay Önöral DDS, PhD(C) https://orcid.org/0000-0002-5264-9376

REFERENCES

1. Ma B, Yue X, Sun Y, Peng L, Geng W. Accuracy of photogrammetry, intraoral scanning, and conventional impression techniques for complete-arch implant rehabilitation: an in vitro comparative study. BMC Oral Health. 2021;21(1):1–9.
2. Mizumoto RM, Yilmaz B, McGlumphy EA, Seidt J, Johnston WM. Accuracy of different digital scanning techniques and scan bodies for complete-arch implant-supported prostheses. J Prosthet Dent. 2020;123(1):96–104.
3. Çakmak G, Yilmaz H, Santos A, Kökat A. Accuracy of different complete-arch digital scanning techniques with a combined healing abutment–scan body system. Int J Oral Maxillofac Implants. 2022;37(1):67–75.
4. Ke Y, Zhang Y, Wang Y, Chen H, Sun Y. Comparing the accuracy of full-arch implant impressions using the conventional technique and digital scans with and without prefabricated landmarks in the mandible: an in vitro study. J Dent. 2023;135(August 2022):104561.
5. Khoshkhahesh M, Enteghad S, Aghasadeghi K, Farzin M, Taghva M, Mosadad SA. Evaluation of the effect of different core substrates on the accuracy of intraoral scanners. Clin Exp Dent Res. 2024;10(3):1–7.
6. Wu HK, Wang J, Chen G, Huang X, Deng F, Li Y. Effect of novel prefabricated auxiliary devices attaching to scan bodies on the accuracy of intraoral scanning of complete-arch with multiple implants: an in-vitro study. J Dent. 2023;138:104702.
7. Menini M, Setti P, Pera F, Pera P, Pesce P. Accuracy of multi-unit implant impression: traditional techniques versus a digital procedure. Clin Oral Investig. 2018;22(3):1253–62.
8. Jeong M, Ishikawa-Nagai S, Lee JD, Lee SJ. Accuracy of impression scan bodies for complete arch fixed implant-supported restorations. J Prosthet Dent. 2023;1–8.
9. Nateghi M, Negahdari R, Molaei S, Barzegar A, Bohlouli S. Comparison of the accuracy of fixture-level implant impression making with different splinting techniques. Int J Dent. 2021;2021:1.
10. Lyu M, Di P, Lin Y, Jiang X. Accuracy of impressions for multiple implants: a comparative study of digital and conventional techniques. J Prosthet Dent. 2022;128(5):1017–23.
11. Baldissara P, Koci B, Messias AM, Meneghello R, Ghelli F, Gatto MR, et al. Assessment of impression material accuracy in complete-arch restorations on four implants. J Prosthet Dent. 2021;126(6):763–71.

12. Huang R, Liu Y, Huang B, Zhang C, Chen Z, Li Z. Improved scanning accuracy with newly designed scan bodies: an in vitro study comparing digital versus conventional impression techniques for complete-arch implant rehabilitation. Clin Oral Implants Res. 2020;31(7):625–33.
13. Rutkunas V, Bilius V, Simonaitis T, Auskalnis L, Jurgilevicius J, Akulauskas M. The effect of different implant impression splinting techniques and time on the dimensional accuracy: an in vitro study. J Dent. 2022;126(October 2021):104267.
14. Yang X, Liu Y, Li Y, Zhao Y, Di P. Accuracy and feasibility of 3D-printed custom open trays for impressions of multiple implants: a self-controlled clinical trial. J Prosthet Dent. 2022;128(3):396–403.
15. Bocklet C, Renne W, Mennito A, Bacro T, Latham J, Evans Z, et al. Effect of scan substrates on accuracy of 7 intraoral digital impression systems using human maxilla model. Orthod Craniofacial Res. 2019;22(S1):168–74.
16. Ashry A, Abdelhamid AM, Ezzelarab S, Khamis MM. Effect of using scan body accessories and inter-implant distances on the accuracy of complete arch implant digital impressions: an in vitro study. J Prosthodont. 2024;(November 2023):1–9.
17. García-Martínez I, Zarauz C, Morejón B, Ferreiroa A, Pradíes G. Influence of customized over-scan body rings on the intraoral scanning effectiveness of a multiple implant edentulous mandibular model. J Dent. 2022;122(March):104095.
18. Pozzi A, Arcuri L, Lio F, Papa A, Nardi A, Londono J. Accuracy of complete-arch digital implant impression with or without scanbody splinting: an in vitro study. J Dent. 2022;119(October 2021):104072.
19. Wu HK, Chen G, Zhang Z, Lin X, Huang X, Deng F, et al. Effect of artificial landmarks of the prefabricated auxiliary devices located at different arch positions on the accuracy of complete-arch edentulous digital implant scanning: an in-vitro study. J Dent. 2024;140(December 2023):104802.
20. Kernen F, Recca M, Vach K, Nahles S, Nelson K, Flügge T. In vitro scanning accuracy using different aids for multiple implants in the edentulous arch. Clin Oral Implant Res. 2022;33(10):1010–20.
21. Roig E, Roig M, Garza LC, Costa S, Maia P, Espona J. Fit of complete-arch implant-supported prostheses produced from an intraoral scan by using an auxiliary device and from an elastomeric impression: a pilot clinical trial. J Prosthet Dent. 2022;128(3):404–14.
22. Llansana F, Guirao S, Kois JC, Revilla-León M. Calibrated splinting framework for complete arch intraoral implant digital scans manufactured by combining milled and additively manufacturing technologies: a dental technique. J Prosthet Dent. 2022;1–7.
23. Guirao S, Llansana F, Button H, Yilmaz B, Kois JC, Revilla-León M. Additively manufactured devices with varying designs and sizes for acquiring initial intraoral implant scans. J Prosthodont. 2023;32(July):181–85.
24. Wu HK, Wang J, Chen G, Huang X, Deng F, Li Y. Effect of novel prefabricated auxiliary devices attaching to scan bodies on the accuracy of intraoral scanning of complete-arch with multiple implants: an in-vitro study. J Dent. 2023;138(June):104702.
25. Dutton E, Ludlow M, Mennito A, Kelly A, Evans Z, Culp A, et al. The effect different substrates have on the trueness and precision of eight different intraoral scanners. J Esthet Restor Dent. 2020;32(2):204–18.
26. Revilla-León M, Jiang P, Sadeghpour M, Piedra-Cascón W, Zandinejad A, Özcan M, et al. Intraoral digital scans—Part 1: influence of ambient scanning light conditions on the accuracy (trueness and precision) of different intraoral scanners. J Prosthet Dent. 2020;124(3):372–78.
27. Braian M, Wennerberg A. Trueness and precision of 5 intraoral scanners for scanning edentulous and dentate complete-arch mandibular casts: a comparative in vitro study. J Prosthet Dent. 2019;122:129-36.e2.
28. Lim J-H, Park J-M, Kim M, Heo S-J, Myung J-Y. Comparison of digital intraoral scanner reproducibility and image trueness considering repetitive experience. J Prosthet Dent. 2018;119:225–32.
29. Revilla-León M, Jiang P, Sadeghpour M, Piedra-Cascón W, Zandinejad A, Özcan M, et al. Intraoral digital scans-Part 1: influence of ambient scanning light conditions on the accuracy (trueness and precision) of different intraoral scanners. J Prosthet Dent. 2020;124:372–78.
30. Revilla-León M, Gohil A, Barmak AB, Gómez-Polo M, Pérez-Barquero JA, Att W, et al. Influence of ambient temperature changes on intraoral scanning accuracy. J Prosthet Dent. 2023;130:755–60.
31. Hayama H, Fueki K, Wadachi J, Wakabayashi N. Trueness and precision of digital impressions obtained using an intraoral scanner with different head size in the partially edentulous mandible. J Prosthodont Res. 2018;62:347–52.
32. Pattamavilai S, Ongthiemsak C. Accuracy of intraoral scanners in different complete arch scan patterns. J Prosthet Dent. 2022;131:155–62.
33. Revilla-León M, Quesada-Olmo N, Gómez-Polo M, Sicilia E, Farjas-Abadia M, Kois JC. Influence of rescanning mesh holes on the accuracy of an intraoral scanner: an in vivo study. J Dent. 2021;115:103851.
34. Revilla-León M, Sicilia E, Agustín-Panadero R, Gómez-Polo M, Kois J. Clinical evaluation of the effects of cutting off, overlapping, and rescanning procedures on intraoral scanning accuracy. J Prosthet Dent. 2023;130:746–54.
35. Button H, Kois J, Barmak A, Zeitler J, Rutkunas V, Revilla-León M. Scanning accuracy and scanning area discrepancies of intraoral digital scans acquired at varying scanning distances and angulations among 4 different intraoral scanners. J Prosthet Dent. 2023;3913:00067.
36. Kaewbuasa N, Ongthiemsak C. Effect of different arch widths on the accuracy of three intraoral scanners. J Adv Prosthodont. 2021;13:205–15.
37. Gan N, Xiong Y, Jiao T. Accuracy of intraoral digital impressions for whole upper jaws, including full dentitions and palatal soft tissues. PLoS One. 2016;11:e0158800.
38. Huang M-Y, Son K, Lee K-B. Effect of distance between the abutment and the adjacent teeth on intraoral scanning: an in vitro study. J Prosthet Dent. 2021;125:911–17.
39. Son K, Lee K-B. Effect of tooth types on the accuracy of dental 3D scanners: an in vitro study. Mater. 2020;13:1744.
40. Chen Y, Zhai Z, Li H, Yamada S, Matsuoka T, Ono S, et al. Influence of Liquid on the Tooth Surface on the Accuracy of Intraoral Scanners: an In Vitro Study. J Prosthodont. 2022;31:59–64.
41. Gómez-Polo M, Ortega R, Sallorenzo A, Agustín-Panadero R, Barmak AB, Kois JC, et al. Influence of the surface humidity, implant angulation, and interimplant distance on the accuracy and scanning time of complete-arch implant scans. J Dent. 2022;127:104307.
42. Ammoun R, Suprono M, Goodacre C, Oyoyo U, Carrico C, Kattadiyil M. Influence of tooth preparation design and scan angulations on the accuracy of two intraoral digital scanners: an in vitro study based on 3-dimensional comparisons. J Prosthodont. 2020;29:201–6.
43. Oh K, Lee B, Park Y-B, Moon H. Accuracy of three digitization methods for the dental arch with various tooth preparation designs: an in vitro study. J Prosthodont. 2019;28:195–201.
44. Park J-M, Kim R-Y, Lee K-W. Comparative reproducibility analysis of 6 intraoral scanners used on complex intracoronal preparations. J Prosthet Dent. 2020;123:113–20.
45. Revilla-León M, Young K, Sicilia E, Cho S-H, Kois J. Influence of definitive and interim restorative materials and surface finishing on the scanning accuracy of an intraoral scanner. J Dent. 2022;120:104114.
46. Dutton E, Ludlow M, Mennito A, Kelly A, Evans Z, Culp A, et al. The effect different substrates have on the trueness and precision of eight different intraoral scanners. J Esthet Restor Dent. 2020;32:204–18.
47. Gómez-Polo M, Donmez MB, Çakmak G, Yilmaz B, Revilla-León M. Influence of implant scan body design (height, diameter, geometry, material, and retention system) on intraoral scanning accuracy: a systematic review. J Prosthodont. 2023;32(September):165–80.
48. Carneiro Pereira AL, Medeiros VR, daFonte Porto Carreiro A. Influence of implant position on the accuracy of intraoral scanning in fully edentulous arches: a systematic review. J Prosthet Dent. 2021;126(6):749–55.
49. Thanasrisuebwong P, Kulchotirat T, Anunmana C. Effects of inter-implant distance on the accuracy of intraoral scanner: an in vitro study. J Adv Prosthodont. 2021;13(2):107–16.
50. Carneiro Pereira AL, Souza Curinga MR, Melo Segundo HV, da Fonte Porto Carreiro A. Factors that influence the accuracy of intraoral

scanning of total edentulous arches rehabilitated with multiple implants: a systematic review. J Prosthet Dent. 2023;129(6):855–62.
51. Elter B, Tak Ö. Effect of substrate adjacent to the scan region on the trueness of four intraoral scanners: an in vitro study. J Dent. 2023;138:1–19.
52. Gintaute A, Papatriantafyllou N, Aljehani M, Att W. Accuracy of computerized and conventional impression-making procedures for multiple straight and tilted dental implants. Int J Esthet Dent. 2018;13:550–365.

How to cite this article: Önöral Ö, Çakır S. Influence of the color of 3D-printed scan aids on the trueness of complete arch digital scans. J Prosthodont. 2026;35:561–73. https://doi.org/10.1111/jopr.13969